ADVANCED FUNCTIONAL MATERIALS
www.afm-journal.de

Lightweight, Thermally Insulating, Fire-Proof Graphite-Cellulose Foam

Chaoji Chen, Yubing Zhou, Weiqi Xie, Taotao Meng, Xinpeng Zhao, Zhenqian Pang, Qiongyu Chen, Dapeng Liu, Ruiliu Wang, Vina Yang, Huilong Zhang, Hua Xie, Ulrich H. Leiste, William L. Fourney, Shuaiming He, Zhiyong Cai, Zhenqiang Ma, Teng Li, and Liangbing Hu**

Foam materials are widely used in packaging and buildings for thermal insulation, sound absorption, shock absorption, and other functions. They are dominated by petroleum-based plastics, most of which, however, are not biodegradable nor fire-proofing, leading to severe plastic pollution and safety concerns. Here, a fire-proofing, thermally insulating, recyclable 3D graphite-cellulose nanofiber (G-CNF) foam fabricated from resource-abundant graphite and cellulose is reported. A freeze-drying-free and scalable ionic crosslinking method is developed to fabricate Cu^{2+} ionic crosslinked G-CNF (Cu-G-CNF) foam with a low energy consumption and cost. Moreover, the direct foam formation strategy enables local foam manufacturing to fulfil the local demand. The ionic crosslinked G-CNF foam demonstrates excellent water stability (the foam can maintain mechanical robustness even in wet state and recover after being dried in air without deformation), fire resistance (41.7 kW m^{-2} vs 214.3 kW m^{-2} in the peak value of heat release rate) and a low thermal conductivity (0.05 W/(mK)), without compromising the recyclability, degradability, and mechanical performance of the composite foam. The demonstrated 3D G-CNF foam can potentially replace the commercial plastic-based foam materials, representing a sustainable solution against the "white pollution".

1. Introduction

Foam materials are in great demand (≈400 million tons per year) in modern society, which are widely used in food, electronics, transportation, and building industries for shock absorption, storage, sound absorption, and thermal insulation.[1–7] However, most commercial foam materials are made of petroleum-based plastics such as polystyrene (PS), polyurethane (PU), and polyvinyl chloride (PVC).[8–10] These petroleum-based plastics are usually environmentally unfriendly, of high-energy consumption, and undegradable in the processes of synthesis, molding and disposal, leading to severe environmental issues.[11–13] Fire safety is another concern regarding the use of these petroleum-based foam materials due to their poor fire resistance. Therefore, developing fire-resistant, shock absorbing, recyclable, and degradable foam materials is in urgent need toward a sustainable society.

Being environmentally friendly and resource-abundant, natural products from the nature provide a potentially sustainable solution as the alternatives to petroleum-based plastics.[14–17] For example, bio-sourced materials, including cellulose,[18] alginate,[19] starch,[20] and chitosan,[21] have been developed into foam materials with potentially better sustainability than the petrochemical counterparts. In particular, cellulose, as the most abundant natural biopolymer on Earth, is considered one of the most promising sustainable resources, and has been widely used in a range of applications including energy storage, electronics, structural materials, and sensors.[22–26] While it remains challenging to assemble cellulose into hybrid structures combining good water stability, fire

C. Chen, Y. Zhou, T. Meng, X. Zhao, D. Liu, R. Wang, H. Xie, S. He, L. Hu
Department of Materials Science and Engineering
University of Maryland
College Park, MD 20742, USA
E-mail: binghu@umd.edu

W. Xie, Z. Pang, Q. Chen, W. L. Fourney, T. Li
Department of Mechanical Engineering
University of Maryland
College Park, MD 20742, USA
E-mail: lit@umd.edu

The ORCID identification number(s) for the author(s) of this article can be found under https://doi.org/10.1002/adfm.202204219.

V. Yang, Z. Cai
Forest Products Laboratory
USDA Forest Service
Madison, WI 53726, USA

H. Zhang, Z. Ma
Department of Electrical and Computer Engineering
University of Wisconsin – Madison
Madison, WI 53706, USA

U. H. Leiste, W. L. Fourney
Department of Aerospace Engineering
University of Maryland
College Park, MD 20742, USA

DOI: 10.1002/adfm.202204219

retardancy, and thermal insulation, which are required in many applications. Graphite, although being nonrenewable, which can be produced from coal formed underground and is widely used to produce graphene or as anode materials in rechargeable lithium-ion batteries, has also been regarded abundant natural resource.[27–30] In addition, graphite is an allotrope of carbon, and it is naturally formed and found in earth that participates in the carbon cycle, which can be recycled to realize the closed-loop utilization of graphite resources. Processing natural resources into foam materials enables fabrication of environmentally-responsible materials. However, the manufacture of foam materials via freeze-drying method generally involves the expensive facilities and intensive energy consumption.[31] Therefore, developing biodegradable foam materials from resource-abundant natural materials through an energy-efficient freeze-drying-free approach is highly required.

Herein, we demonstrate the scalable, freeze-drying-free fabrication of a 3D graphite-cellulose nanofiber (G-CNF) foam as a new generation of recyclable, degradable, fire-proofing, and thermally insulating foam material via an ionic crosslinking assisted ambient drying strategy (**Figure 1**).[32,33] Graphite flakes can be exfoliated in aqueous environment using only CNF as the dispersing agent. The resulting suspension is stable for a long duration of time (>6 months) and features high viscosity and shear-thinning behavior, which enables it to be processed facilely. To reduce the cost and enable scale-up manufacturing by avoiding using freeze-drying method, we developed a direct foam formation strategy via ionic crosslinking (Figure 1a). The adjacent cellulose chains can be crosslinked by Cu^{2+} ions through electrostatic interaction, which contributes to 3D ionic crosslinking networks among cellulose nanofibers (Figure 1b). Therefore, the wet G-CNF foams can self-stand and be dried at ambient conditions with minimum shrinkage. As the energy-intensive freeze-drying process is avoided, the manufacturing cost is substantially reduced, and scaling-up capability is greatly improved (Figure 1c,d). In addition, the Cu^{2+} crosslinked G-CNF (referred to as Cu-G-CNF hereafter) foams demonstrated excellent water stability, fire resistance and thermal insulation, without compromising the recyclability, degradability, and mechanical performance of the composite foam. Such a process can be potentially scaled up by adapting the mature techniques from pulp and foam industries. In addition, the direct foam formation approach holds great promise to produce G-CNF foams on-demand locally (where the foam will be used), avoiding the long-distance transportation of final foam product (Figure 1e). Note that cellulose can be reused or naturally decomposed into glucose via enzyme-assisted hydrolysis,[34,35] while the chemically inert graphite can be recycled and go back to the carbon cycle, which is naturally environmentally friendly,[36,37] in sharp comparison with the non-degradable petroleum-based plastics.

2. Results and Discussions

2.1. Scalable Fabrication and Hierarchical Structure

Graphite-CNF slurry was first prepared for direct foam formation via ionic crosslinking. The CNF made from waste plant biomass is mixed with graphite flakes in water by sonication treatment. The sonication treatment helps accelerate the insertion of CNF into graphite and promotes the exfoliation of bulk graphite powders into smaller and thinner flakes (Figure S1, Supporting Information). The initial as-prepared graphite-CNF slurry is a fluid with tunable solid concentrations of 2 to 30 wt.%. The cellulose-graphite slurry is stirred with sodium dodecyl sulfate (SDS) at 2000 rpm to generate quantities of stable air bubbles. Then the slurry full of bubbles is immersed in the Cu^{2+} ions solution together with mold and forms self-supporting wet foams. Negative-charged cellulose chains are exposed in Cu^{2+} ions solution, the adjacent two cellulose chains can be crosslinked by Cu^{2+} ions through electrostatic attraction, contributing to 3D ionic crosslinking networks among cellulose chains. Therefore, the cellulose chains are locked, and the aqueous cellulose-graphite foams can self-stand. Due to the 3D ionic crosslinking networks, the Cu^{2+} crosslinked G-CNF (Cu-G-CNF) foams can be obtained by air drying. By avoiding the freeze-drying process, the manufacturing cost can be largely reduced and the scaling-up capability greatly improved. As shown in Figure 1c,d, large scale slurry (up to several gallons) and foam (60 cm × 20 cm × 5 cm in size) can be readily manufactured via the direct foam formation method.

The lightweight Cu-G-CNF foam with a density of 0.040 ± 0.005 g cm^{-3} possesses a porous and hierarchical structure (**Figure 2**a). At the molecular-scale, CNF attaches to the graphite flakes through the interaction between its hydrophobic sites and the hydrophobic plane of the graphite, as well as hydrogen bonding between the CNF hydroxyl groups and the defective edges of the graphite flakes. At the nano-scale the CNFs are well aligned; the CNF fibers are terminated with functional groups such as —OH and —COOH. These hydrophilic functional groups cause the graphite flakes to disperse well in water due to the electrostatic repulsion forces between different flakes. At the micro-scale the microfibers are compactly intertwined; At the macro-scale, the CNF-coated graphite flakes form a 3D structure. SEM observation of a piece of the dry Cu-G-CNF foam revealed a homogeneous interior porous structure, with an average pore size of ≈200 µm (Figure 2b; Figure S2a,b, Supporting Information) and thin cell walls with a thickness of 1–2 µm (Figure 2c; Figure S2c,d, Supporting Information). Copper element distributed uniformly in all outer and inner pore walls of the Cu-G-CNF foam through the energy-dispersive X-ray (EDX) spectrum (Figure 2d; Figure S3, Supporting Information). And the slight decrease and offset of $-COO^-$ peak (1604 cm^{-1}) in FT-IR spectra suggests that the bonding between Cu^{2+} and -COO^- on cellulose nanofibers are formed by electrostatic attraction, contributing to a porous yet robust structure (Figure 2e).

In order to explain the formation process of hydrogen bonding among graphite and CNF, the full molecular dynamics simulations using the ReaxFF potential[38] are implemented in the Large-scale Atomic/Molecular Massively Parallel Simulator (LAMMPS) simulation package.[39] Same with the experimental conditions, the mass ratio of graphite and cellulose is set as 1:1. The further details of the simulation are illustrated in the atomistic modeling (Figure 2f–i;

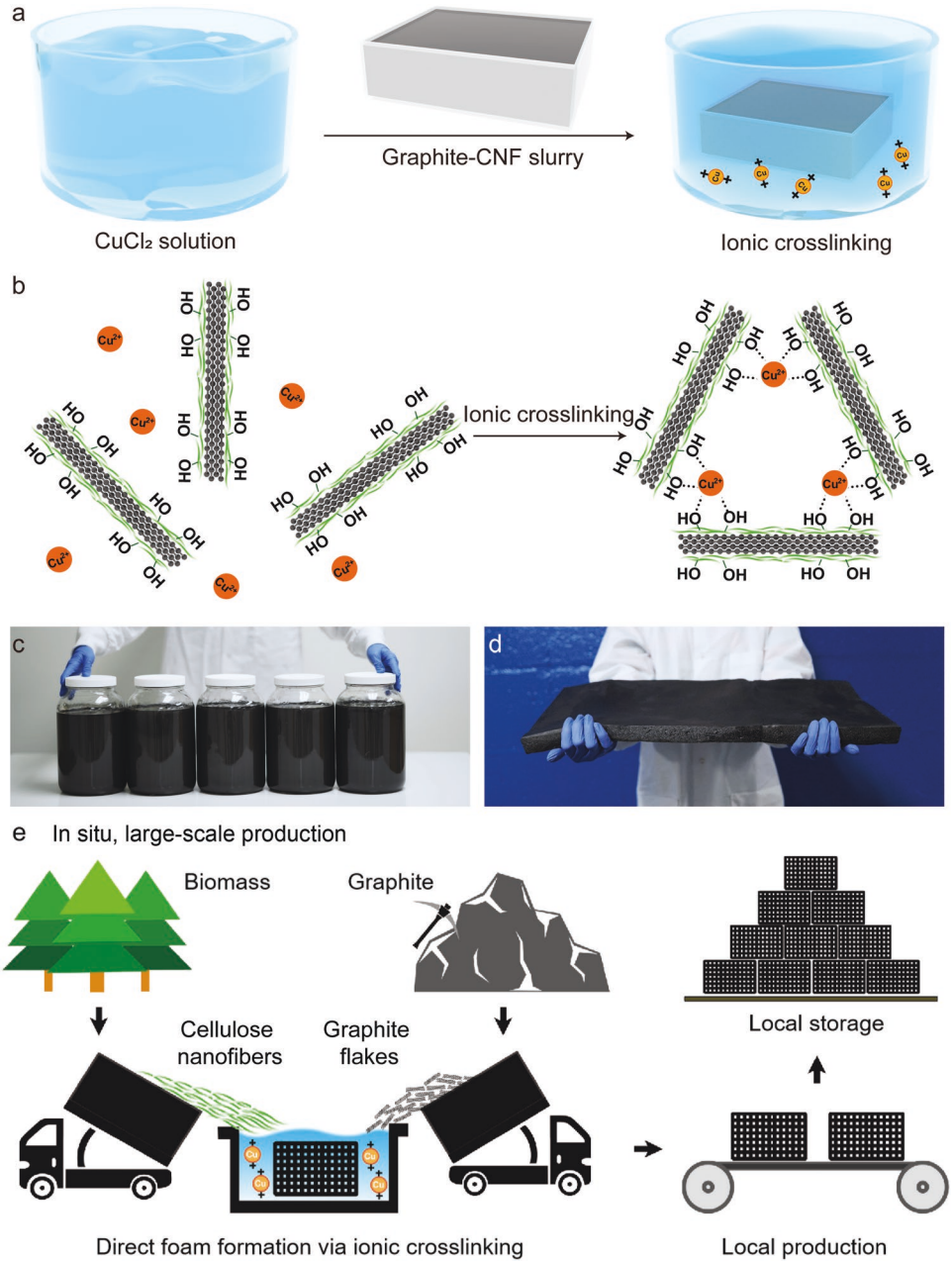

Figure 1. In situ, large-scale production of Cu-G-CNF foams via a freeze-drying-free ionic crosslinking method. a,b) Schematic to show the fabrication process of Cu-G-CNF foam by Cu^{2+} ionic crosslinking. c) Large-volume G-CNF slurries produced by sonication, one gallon per bottle. d) A large scale (60 cm × 30 cm × 5 cm) G-CNF foam after air dry. e) The schematic to show the potential application of in situ, large-scale production. The direct foam formation approach via ionic crosslinking treatment holds great promise to produce G-CNF foams on-demand locally (where the foam will be used), avoiding the long-distance transportation of final foam product.

Figure S4, Supporting Information). Figure 2f,g shows the atomistic structures of graphite foam (G foam) and G-CNF foam constructed with graphite flakes. The inter-flake interactions of graphite flakes are Van der Waals forces and there exists a large amount of hydroxyl groups in the edges of flakes. In the formation of G foam, only part of hydroxyl groups can form the hydrogen bonds due to the orientation of graphite flakes (Figure 2h upper). In contrast, cellulose chains wrap around the graphite flakes (Figure 2h bottom). Such a hybrid material structure significantly promotes hydrogen bonding formation (Figure 2i), which in turn facilitates the formation of foams. To investigate the dependence of the thickness of graphite flakes, the formation process of foams with three and five graphene layers is constructed (Figure S4, Supporting Information). The stability of foams has a negative relationship with the thickness of graphite flakes, which means the thinner the graphite flake is, the more stable the foam is.

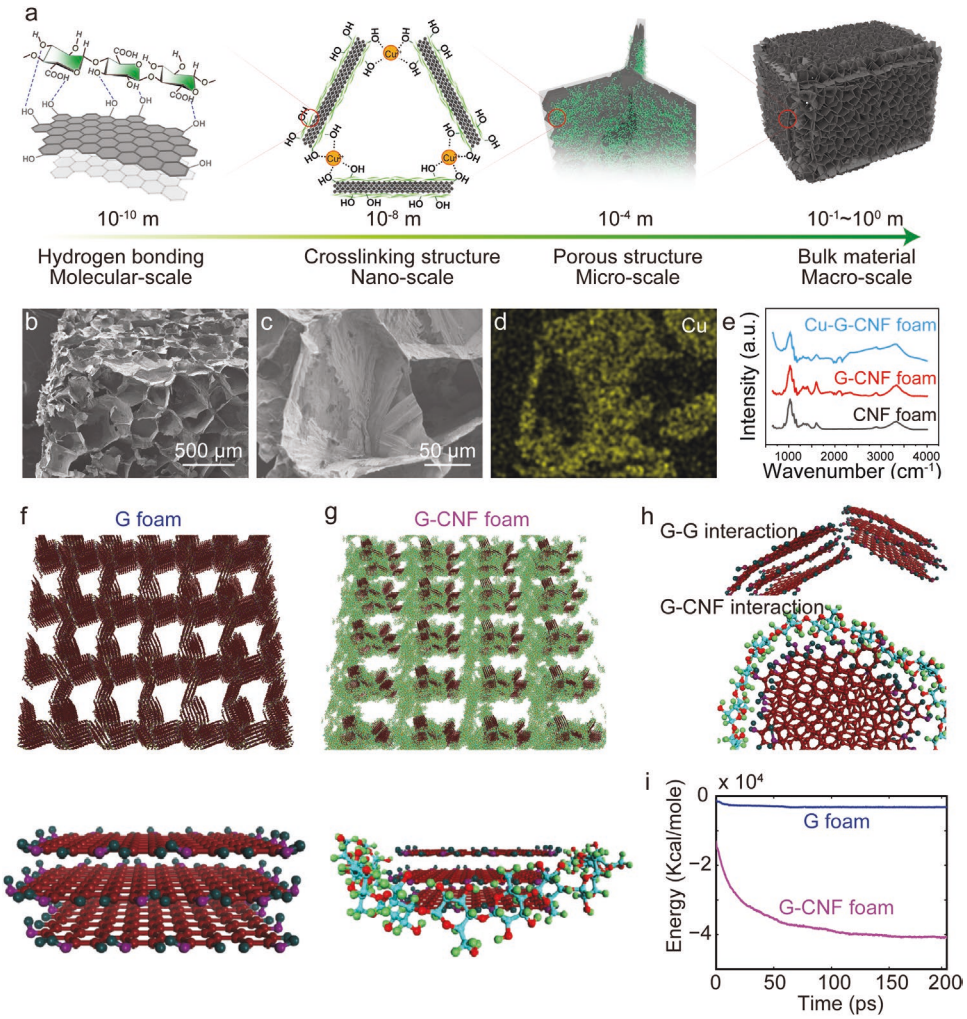

Figure 2. The scalable manufacture of G-CNF foam by Cu^{2+} ionic crosslinking. a) Hierarchical structure of the Cu^{2+} crosslinked G-CNF foam at various length scales. b) SEM image of the microstructure of the Cu-G-CNF foam. c) High-magnification SEM image of the Cu-G-CNF foam. d) EDX elemental map of copper in the Cu-G-CNF foam shown in (c). e) The FT-IR spectrum of the CNF, G-CNF, and Cu–G-CNF foams. Atomistic simulations of the interactions between graphite flakes and cellulose: f) Atomistic structure of G foam constructed with three layers of graphene; g) Atomistic structure of G-CNF foam constructed with three layers of graphene and cellulose molecular chains. Brown and Green atoms represent the graphite flakes and cellulose molecular chains, respectively; h) Interaction between graphite flakes and cellulose molecular chains; i) Variation of hydrogen bonding energy as the function of time in the formation process of foam with and without cellulose. The hydrogen bonding energy increases more than ten times after adding the CNF matrix.

2.2. Mechanical Properties

Such a porous and hierarchical structure is desirable for load bearing and shock energy absorption, which are critical for packaging and building applications as well. In this context, we further evaluated the compressive and shock energy absorption mechanical properties of the G-CNF and Cu-G-CNF foams and compared them with pure CNF and commercial PS foam. As shown in Figure S5 (Supporting Information), the G-CNF foam showed a higher compressive strength (2.2 MPa) than the commercial plastic PS foam (1.11 MPa). The crosslinked Cu-G-CNF foam showed a comparable compressive strength with the plastic PS foam. The hydrogen bonding between the graphite and CNF offers the high compressive strength, while there is the weak connection among the PS microspheres of the commercial plastic PS foam.

A home-made drop tower was used in order to test different materials during impact and evaluate their energy absorbing performance (see Supporting Information for details). Five groups of specimens, namely, aluminum, PS foam, CNF-foam, G-CNF-foam, and Cu-G-CNF-foam, were tested using the configuration shown in **Figure 3**a, of which the velocity of each component was derived from the slope of the linear time-displacement relation recorded by a high speed camera (Figure 3c; Figure S6, Supporting Information). The averaged energy absorbed by four types of foams are listed in Figure 3b and Table S1 (Supporting Information). The G-CNF foam shows higher shock absorption energy than pure CNF foam and PS foam. Further ionic crosslinking leads to higher

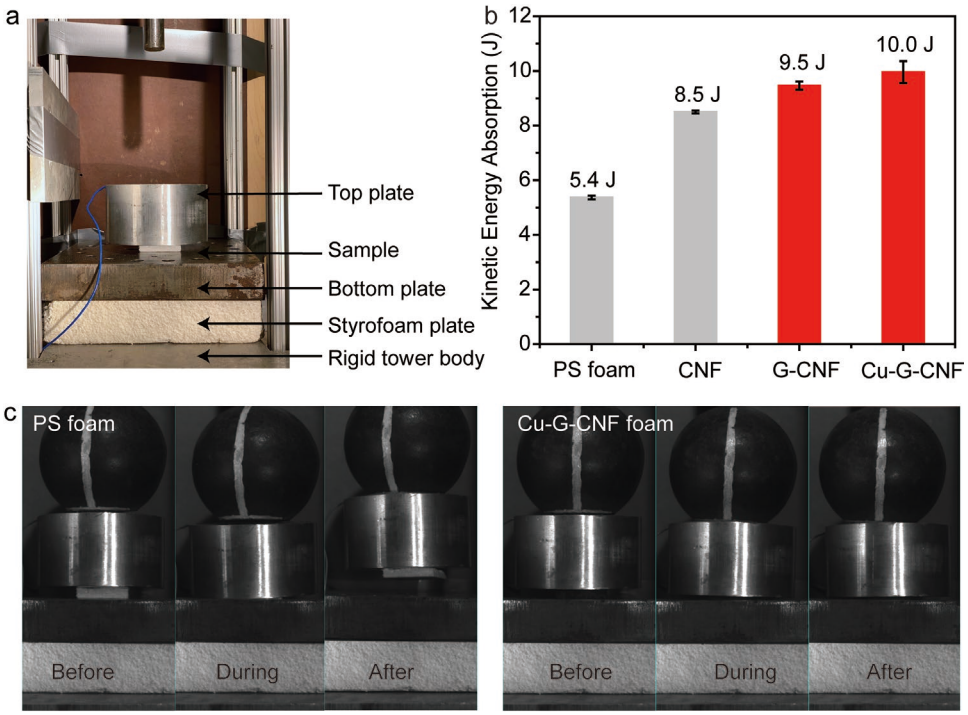

Figure 3. Kinetic Energy Absorption of PS foam, CNF foam, G-CNF foam, and Cu-G-CNF foam. a) Photograph of the drop tower assembly with multiple components including a solid frame, a top plate, a bottom plate, a Styrofoam cushion, and below that a rigid tower bottom plate. b) Kinetic Energy Absorption of PS foam, CNF foam, G-CNF foam, and Cu-G-CNF foam. c) Photographs captured by high-speed camera during the tests.

shock absorption energy of ≈10 J. These results suggest that the hybridization of large-sized graphite flakes and the ionic crosslinking both contribute to the improvement of mechanical shock absorption of the graphite-CNF composite foam.

2.3. Fire Retardancy and Thermal Property

Fire safety is a critical property for foam materials, which has been a long-standing challenge for traditional foam materials like PS.[40,41] The fire-retardant behavior of the PS foam, CNF foam, graphite-CNF foam, and Cu-G-CNF foam was further assessed with the vertical burning test (UL-94), as shown in **Figure 4**a–d. It was observed that both PS and CNF foams can be easily ignited, and the flame spreads rapidly to the top of the sample within 10 s. Finally, the whole samples of PS and CNF foams were ruined with little char residue left. For the G-CNF foam, the flame extinguished when the burner source was removed, indicating that the existence of the graphite in the G-CNF foam retarded the flame burning on the CNF. However, the smoldering phenomena occurred that burned out the sample finally. By contrast, the Cu-G-CNF foam exhibited excellent flame retardancy and the flame extinguished immediately when the burner source was removed. The above results proved that Cu-G-CNF foam displayed superior fire-retardant properties, which was mainly originated from the synergistic effect between graphite and Cu^{2+} during the combustion process.

To examine the fire-retardant behavior of the Cu-G-CNF foam more quantitatively, cone calorimeter test (CCT) was performed. Figure 4e depicted the heat release rate (HRR) and total heat release (THR) curves as a function of time from foam samples, and the corresponding results (THR, peak value of HRR (HRR_{peak})) were also displayed in Figure S7 (Supporting Information). It is generally known that HRR value (especially HRR_{peak}) is an important parameter that can be served as the main indicator of the fire-safety properties of materials. It was observed that HRR_{peak} of PS foam was up to 214.3 kW m^{-2}. For the CNF foam, HRR_{peak} decreases to 121.6 kW m^{-2}, corresponding to a 43.3% reduction in contrast to that of the PS foam. The G-CNF foam exhibited a further reduction in HRR_{peak} to 69.4 kW m^{-2}, since graphite played an important role in physical barrier effect. The Cu-G-CNF foam showed the lowest HRR_{peak} value (41.7 kW m^{-2}), corresponding to an 80.5% reduction in contrast to that of the PS foam, which confirmed the excellent flame retardant effect (Figure 4f). It is notable that the earlier heat release of CNF series foams is ascribed to the early decomposition of unstable structure (i.e., glycosidic bond) in CNF.[42,43] Similarly, the reduction in THR for Cu-G-CNF foam is up to 61.0% compared with that of PS foam (2.96 MJ m^{-2} vs.7.59 MJ m^{-2}). The significantly reduced THR of the Cu-G-CNF foam indicated the lower heat generated from the combustion of flammable volatiles escaped from the foam samples.

The above results clearly verified that the synergistic effect between graphite and Cu^{2+} endowed the Cu-G-CNF foam with excellent fire-retardant properties. The existence of the thermally stable graphite effectively enhanced the thermal stability of Cu-G-CNF foam, thus contributing to the improved fire retardancy of the foam material.[44–46] Moreover, the graphite in Cu-G-CNF foam can also serve as the char former to facilitate

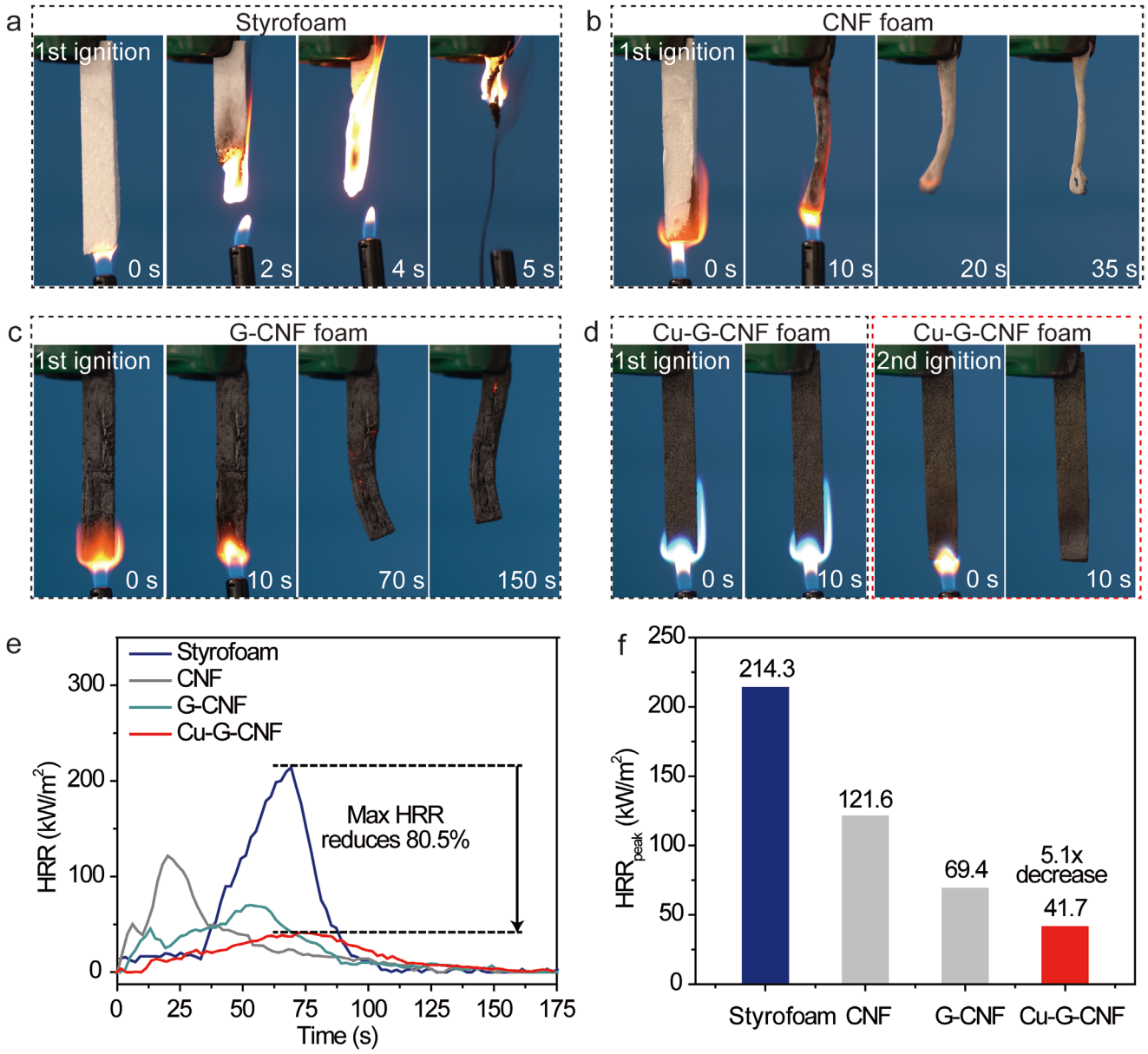

Figure 4. Fire retardancy and thermal property of the Cu-G-CNF foam. The digital images of the vertical burning test on the a) PS, b) CNF, c) G-CNF, and d) Cu-G-CNF foams. e) *HHR* versus time, f) HRR_{peak} values of PS, CNF, G-CNF, and Cu-G-CNF foams.

the formation of dense char layer upon burning. In addition, the Cu^{2+} in Cu-G-CNF is able to catalyze the formation of compact char in the combustion process, and the stable char layer serves as a barrier between air and the cellulose interior, which further decreased the release of gaseous products of Cu-G-CNF foam.[47,48] Therefore, the effective synergistic effect of graphite and Cu^{2+} enabled the superior flame retardancy of Cu-G-CNF foam. In brief, the Cu-G-CNF foam demonstrates the best safety against fire among all tested foams.

The Cu-G-CNF foam demonstrates a low thermal conductivity of 0.05 W m^{-1} K^{-1} (Figures S8 and S9, and Table S2, Supporting Information), which attributes to its high porosity structures (≈97%) and tortuous solid conduction path. Since the pore size (100–500 µm) is much <4 mm, air convection inside the pores is completely suppressed.[49] The measured thermal conductivity is slightly higher than the conventional petroleum-based insulation materials such as expanded polystyrene, which is reasonable given its high graphite content of ≈50 wt.%. The combination of high mechanical strength, good fire retardancy and low thermal conductivity positions the Cu-G-CNF foam as a promising candidate for the replacement of petroleum-based foam materials.

2.4. Water Stability, Recyclability, and Degradability

The stability against moisture and water is another key factor for green and sustainable foam materials. Both CNF and

Figure 5. The demonstration of the water stability, recyclability, and degradability of the Cu-G-CNF foam. Water stability of the CNF (left), G-CNF (middle), and Cu-G-CNF (right) foams: Shape retain ability in water, photographs of the foams in a) fully wetted state, and b) after drying. The CNF foam and G-CNF foam shrink significantly, while the Cu-G-CNF foam can retain its shape well. c) Photographs of the CNF foam (left), G-CNF foam (middle), and Cu-G-CNF foam (right) soaked in water. d) Behaviors after compression. CNF and G-CNF foams were easily damaged under the same pressure (the poise is 500 g); on the contrary, crosslinked G-CNF foam kept its 3D structure. e) The recyclability of the Cu-G-CNF foam. f) The degradability of the PS, CNF, graphite-CNF, and Cu-G-CNF foams.

G-CNF foams demonstrated inferior performance due to the hydrophilic and water absorbing nature of cellulose without crosslinking. As CNF features abundant oxygenated functional groups, the fibers have a strong tendency to absorb water and swell. Swelling occurs as water wets the CNF surfaces and continues to fill and create more space between the fibers. The swollen CNF and G-CNF foams tended to shrink during drying (**Figure 5**a,b). The Cu^{2+} crosslinking strategy can significantly improve the water stability of the graphite-cellulose foam. On the one hand, the crosslinked graphite-cellulose foam can not only maintain the structure unchanged when immersed in water, but also the mechanical strength. On the other hand, after drying in air, no structural deformation (e.g., shrinkage) was observed, suggesting its excellent structural stability upon water removal (e.g., after being exposed to water and dried naturally in air, see Figure 5a,b). In addition, the Cu^{2+} crosslinked G-CNF foam shows another advantage of being able to sustain certain compressive loading even at fully wet state due to the 3D strong ionic crosslinked network (Figure 5c,d), which is an additional benefit for foam material application (that is, even being wet, the foam material can remain functional). The above results suggest that the water stability of our graphite-cellulose foam material is much better than pure cellulose foam benefiting from the graphite hybridization and ionic crosslinking. And the combination of low water absorption/swelling degree, good recovery after being dried, and excellent retention of mechanical strength even at wet state confirms that water stability should not be an issue for our graphite-cellulose foam material. The G-CNF and Cu-G-CNF foams are stable under moisture attack (Figures S10 and S11, Supporting Information). For example, after being exposed to 98% RH for 166 h, the change in dimensions of the CNF foam, G-CNF foam, and Cu^{2+} crosslinked G-CNF foam is modest (<3% increase in thickness) (Figure S10a–c, Supporting Information). The G-CNF foam

without cross-linking absorbed 14% water after 166 h, whereas the CNF foam absorbed 19% water within the same time period (Figure S10d, Supporting Information). The Cu^{2+} crosslinked G-CNF foam absorbed ≈65% water due to the hygroscopic of residual copper salt on the surface. More attractively, the Cu-G-CNF foam demonstrated outstanding stability in both acid and alkaline solution, presenting great potential to diverse application of the foam material (Figures S12 and S13, Supporting Information).

We also demonstrated the recyclability and degradability of Cu-G-CNF foam and crosslinked G-CNF foam materials. Currently, the recycling method of waste PS foam is to crush, melt, and then process it into new PS materials. However, for the above recycling method, the raw materials are not completely crushed, the melting temperature is not controlled uniformly, and the impurities mixed in the raw materials cannot be avoided, which leads to relatively low production efficiency and equipment damage due to the existence of impurities. Thus, a new recycling method is imminent. In this work, the Cu-G-CNF foams can be back to slurry through the acid and alkali treatment to remove the Cu^{2+} ions and reconstruct uniform slurry (Figure 5e). For CNF and G-CNF foams, uniform dispersion slurries of CNF and graphite-CNF can be obtained through the fast re-dispersion of the used CNF and G-CNF foam in water in seconds under stirring. The recycled CNF and graphite-CNF slurry can be used to fabricate CNF and G-CNF foams, enabling a closed cycle of repeating use. The CNF and G-CNF foams can also be converted into a new foam with new designed shape and size for another propose via the re-dissolving and re-printing process. For Cu-G-CNF, the graphite-CNF slurry can be easily and completely reused for direct foam formation via ionic crosslinking. The recycled Cu-G-CNF foam delivered a compressive stress (0.485 MPa), comparable to the original Cu-G-CNF foam and PS foam (Figure S14, Supporting Information). The recycled Cu-G-CNF foam presented similar thermal conductivity (0.061 W m^{-1} k^{-1}), and density (0.040 ± 0.005 g cm^{-3}) to the original foam. These results indicated good recyclability of the Cu-G-CNF foam, realizing closed-loop material recycling with economic feasibility.

The degradation properties of the graphite-cellulose foams were evaluated by outdoor exposure to the natural ambient environment and fungi degradation. The PS foam, CNF foam, G-CNF foam, and Cu-G-CNF foam with similar volume were placed on the lawn in natural ambient environment (Figure 5f). After 60 days, the volume of CNF foam, G-CNF foam and Cu-G-CNF foam reduced obviously, while the commercial plastic foam keeps unchanged. The CNF foam and G-CNF foam continued shrinking and disappeared after 180 days, suggesting an excellent degradability without adding harm to the environment. Of note, during biodegradation of the Cu-G-CNF foam, copper may be released to the environment, possibly leading to potential harm to the environment and human health. The biodegradation behavior, especially the potential copper releasing and its harm to the environment and human bodies needs further investigation. In sharp contrast, the commercial plastic PS foam maintained the original shape, barely indicating any appreciable degradability. For fungi degradation test, two wood decay fungi, Postia placenta (Fr.) M.Lars and Lomb. (MAD 698) and Phanerochaete chrysosporium (ME 461), and a mixed mold fungi composed of Aspergillus niger 2.242, Penicillin chrysogenum PH02 and Trichoderma atraviride ATCC 20476 were tested on four types of foams made from pure CNF, composite of graphite and CNF (G-CNF), composite of Cu^{+} crosslinked graphite and CNF (Cu-G-CNF), and PS (See Experimental Section for details about fungi preparation). The foams samples were cut into 1 inch cubic and tested using the fungi for 12 weeks period. Table S3 (Supporting Information) summarizes the average weight loss percentage of each sample with standard deviation. Among the tested four types of foam samples (i.e., CNF, G-CNF, Cu-G-CNF, and PS), Cu-G-CNF demonstrated the highest weight loss, suggesting excellent fungi degradation capability of this sample.

3. Conclusion

In conclusion, we develop a lightweight, robust, water-stable, recyclable, and degradable 3D graphite-cellulose foam material via a freeze-drying-free ionic crosslinking method. The G-CNF slurry maintains high apparent viscosity as well as good storage and loss moduli stability, which enable the direct mold-forming production of 3D foam products. Owing to the electrostatic interaction between Cu^{2+} ions and negatively-charged cellulose, 3D crosslinking network of interconnected cellulose chains with open microcellular structure are established. The Cu^{2+} crosslinked G-CNF scaffold can form free-standing porous structures and prevent from collapsing without any stabilization options during air drying. A large-scale (60 cm × 30 cm × 5 cm) Cu-G-CNF foam can be readily manufactured through the direct foam formation method. Moreover, the synergistic effect between Cu^{2+} and graphite endowed Cu-G-CNF foam composites with high flame-retardant properties and long-term water stability, suggesting a better safety. Due to the reversible bonding mechanism (i.e., hydrogen bonding) in the Cu-G-CNF composite, an excellent degradability and recyclability can be achieved. In addition, the graphite-cellulose foam demonstrates better shock energy absorption capability than the commercial PS foam and excellent thermal insulation (with a low thermal conductivity of 0.05 W m^{-1} K^{-1}), mainly owning to its porous, 3D ionic crosslinked network structure. The low-cost, efficient, and scalable method can also be extended to the local manufacturing of graphite-cellulose foams on islands or in remote areas, which can be considered a promising alternative for large-scale production of foam materials. Our strategy of combining resource-abundant and cost-effective materials (i.e., graphite and cellulose) through reversible hydrogen bonding represents a promising direction for developing recyclable and degradable foam materials.

4. Experimental Section

Graphite/CNF Slurry Preparation: The cellulose nanofiber (CNF) was prepared from the wood pulp via TEMPO-mediated oxidation method according to the previous report.[50] The graphite flakes were purchased from the Asbury Carbons, co Ltd. and used without any treatment. The graphite was mixed with the CNF dispersion with the weight ratio of

1:1 under sonication by ultrasonic cell disruptor for 1 h to obtain the uniform slurry with the concentration of 2 wt.%.

The graphite/CNF slurries with differential concentration of 4, 8, 10, 20, and 30 wt.% were prepared through evaporating different amount of solvent (water) on hot plate with continuously stirring.

Fabrication Process of Graphite-Cellulose Foams by Ionic Crosslinking: Sodium dodecyl sulfate (SDS) (Sigma-Aldrich, ⩾99.0%) and copper (II) chloride ($CuCl_2$) (Sigma-Aldrich, ⩾99.0%) were used to form stable bubbles and ionic crosslinking respectively. The SDS was added into the graphite-cellulose slurry and stirred with 2000 rpm for almost 5 min until no more bubbles were generated. Then the graphite-cellulose slurry full of air bubbles was immersed into $CuCl_2$ solution (0.05 mol L^{-1}) for molding and crosslinking. Finally, the wet cellulose-graphite foams were removed from the $CuCl_2$ solution and dry in air. The content of Cu in the final Cu-G-CNF foam was 2.28% by an investigation of inductively coupled plasma mass spectrometry (ICP-MS).

Characterizations: A scanning electron microscope (Hitachi SU-70) was used to characterize the morphologies and the structures of the G-CNF foam. A Thermo Nicolet NEXUS 670 FT-IR was used to measure the FT-IR spectrums of CNF and G-CNF.

Mechanical Properties Test: A single column tabletop model testing system (Instron, USA) was used to perform the tensile mechanical tests of G-CNF foam and Plastic foam. The mechanical compression tests were performed using RSA III dynamic mechanical analyzer (TA instrument) at a constant loading speed of 4 mm min. The sample was cut into cube with a length of 10 mm by a razor blade. All samples were tested under the same conditions in ambient environment.

Drop Tower Test: A drop tower was used in order to test different materials during impact and evaluate their energy absorbing performance. The drop tower consists of a solid frame that accommodates a guiding rod for the drop weight, a top plate which gets directly impacted by the drop weight, a bottom plate, below the bottom plate a Styrofoam cushion, and below that a rigid tower bottom plate. All tests were performed, using an identical test procedure. A 6.724 kg drop weight was dropped from a height of 30 cm for impacting the top plate of the dimensions ($D \times H$) 150 mm × 70 mm. The aluminum plate had a mass of 2.31 kg. Below the top plate, the specimen of interest was placed and centered between the top plate and the bottom plate. The specimens were of the dimension ($L \times W \times H$) of 50 mm × 50 mm × 10 mm. The specimens used were made out of aluminum (as reference to calculate the energy dissipation in the whole system), PS foam, CNF-foam, G-CNF-foam, and Cu-G-CNF-foam. Each type of specimen was tested twice. The bottom plate was made out of steel and had the mass of 15.03 kg. The Styrofoam plate between the bottom plate and the ridged tower body plate was used as an impedance mismatch for sensors utilized and performed as a security device in case of overloading the plates.

Stability Test against Moisture: The CNF foam, G-CNF foam, and Cu-G-CNF foam with dimensions of ≈40 mm length by 30 mm width by 15 mm thickness were prepared. The samples were put into the humidity chamber (LHS-150HC-II, set to 25 °C, 98% RH) and measured at regular intervals. The dimensions of the samples after various intervals in the humidity chamber were recorded.

Fire-Retardant Properties: A vertical burning test was conducted on a UL-94 flammability meter (Fire Testing Technology Co. Ltd., UK) (sheet dimension was 130 × 13 × 3.2 mm^3) according to ASTM D3801-10.

The combustion behavior of foam samples (sheet dimension was 100 × 100 × 5.0 mm^3) were evaluated by cone calorimetry (Fire Testing technology, FTT, UK) according to ISO5660 (external heat flux = 35 kW m^{-2}). The measurement for each sample was repeated in triplicate.

Supporting Information

Supporting Information is available from the Wiley Online Library or from the author.

Acknowledgements

The authors acknowledge the financial support of Trinity Industries, Inc. for this research. The author acknowledge the support of the National Science Foundation, USA (Grants CMMI # 1936452). The author acknowledge the support of the Maryland Nanocenter, its Surface Analysis Center, and AIMLab. The author acknowledge the University of Maryland supercomputing resources (https://hpcc.umd.edu) and Maryland Advanced Research Computing Center (MARCC) made available for conducting the research reported in this paper.

Conflict of Interest

The authors declare no conflict of interest.

Author Contributions

C.C., Y.Z., W.X., and T.M. equally contributed to this work. L.H., C.C., and Y.Z designed the experiments. Y.Z. and W.X. contributed to the synthesis. Y.Z., U.L., W.L.F., Q.C., and T.L. designed and carried out the impact absorption tests. Y.Z. provided characterizations via SEM. W.X. contributed to the test of fire retardant properties. S.H. contributed to the FT-IR spectrum measurement. Z.P. and T.L. contributed to the mechanical modeling and the corresponding analysis. X.Z. contributed to the thermal property measurements and analysis. V.Y., Z.C., H.Z., and Z.M. contributed to the fungi degradation tests. C.C., Y.Z., L.H., and T.L. collectively analyzed all data and wrote the paper. T.M. contributed to material fabrication and characterization during revision. All authors commented on the final manuscript.

Data Availability Statement

The data that support the findings of this study are available from the corresponding author upon reasonable request.

Keywords

bio-composites, cellulose, degradability, fire retardants, foam materials

Received: April 22, 2022
Revised: October 29, 2022
Published online: December 8, 2022

[1] O. G. Piringer, A. L. Baner, *Plastic packaging materials for food: barrier function, mass transport, quality assurance, and legislation*, John Wiley & Sons, Hoboken, New Jersey **2008**.
[2] S. Mecking, *Angew. Chem., Int. Ed.* **2004**, *43*, 1078.
[3] O. Hauenstein, S. Agarwal, A. Greiner, *Nat. Commun.* **2016**, *7*, 11862.
[4] B. P. Jelle, *Energy Build.* **2011**, *43*, 2549.
[5] M. S. Al-Homoud, *Build. Environ.* **2005**, *40*, 353.
[6] T. Li, J. Song, X. Zhao, Z. Yang, G. Pastel, S. Xu, C. Jia, J. Dai, C. Chen, A. Gong, F. Jiang, Y. Yao, T. Fan, B. Yang, L. Wagberg, R. Yang, L. Hu, *Sci. Adv.* **2018**, *4*, eaar3724.
[7] S. Bhatnagar, M. Hanna, *Trans. ASAE* **1995**, *38*, 567.
[8] K. W. Suh, C. P. Park, M. J. Maurer, M. H. Tusim, R. D. Genova, R. Broos, D. P. Sophiea, *Adv. Mater.* **2000**, *12*, 1779.
[9] D. Feldman, *Materials for Energy Efficiency and Thermal Comfort in Buildings*, CRC Press, Boca Raton, FL **2010**.

[10] M. Dopico-García, J. López-Vilariñó, M. González-Rodríguez, *J. Agric. Food Chem.* **2007**, *55*, 3225.
[11] S. B. Borrelle, J. Ringma, K. L. Law, C. C. Monnahan, L. Lebreton, A. McGivern, E. Murphy, J. Jambeck, G. H. Leonard, M. A. Hilleary, M. Eriksen, H. P. Possingham, H. De Frond, L. R. Gerber, B. Polidoro, A. Tahir, M. Bernard, N. Mallos, M. Barnes, C. M. Rochman, *Science* **2020**, *369*, 1515.
[12] M. Haward, *Nat. Commun.* **2018**, *9*, 667.
[13] R. Geyer, J. R. Jambeck, K. L. Law, *Sci. Adv.* **2017**, *3*, 1700782.
[14] L. Chen, S. Wang, S. Wang, C. Chen, L. Qi, L. Yu, Z. Lu, J. Huang, J. Chen, Z. Wang, X.-W. Shi, Z. Song, H. Liu, C. Chen, *ACS Nano* **2022**, *16*, 16414.
[15] H. Zhu, W. Luo, P. N. Ciesielski, Z. Fang, J. Zhu, G. Henriksson, M. E. Himmel, L. Hu, *Chem. Rev.* **2016**, *116*, 9305.
[16] C. Xu, R. A. D. Arancon, J. Labidi, R. Luque, *Chem. Soc. Rev.* **2014**, *43*, 7485.
[17] R. J. Moon, A. Martini, J. Nairn, J. Simonsen, J. Youngblood, *Chem. Soc. Rev.* **2011**, *40*, 3941.
[18] S. J. Eichhorn, A. Etale, J. Wang, L. A. Berglund, Y. Li, Y. Cai, C. Chen, E. D. Cranston, M. A. Johns, Z. Fang, G. Li, L. Hu, M. Khandelwal, K. Y. Lee, K. Oksman, S. Pinitsoontorn, F. Quero, A. Sebastian, M. M. Titirici, Z. Xu, S. Vignolini, B. Frka-Petesic, *J. Mater. Sci.* **2022**, *57*, 5697.
[19] T. Vincent, L. Dumazert, L. Dufourg, C. Cucherat, R. Sonnier, E. Guibal, *J. Appl. Polym. Sci.* **2018**, *135*, 45868.
[20] C. Badouard, F. Bogard, C. Bliard, M. Lachi, B. Abbes, G. Polidori, *Constr. Build. Mater.* **2021**, *302*, 124142.
[21] N. Mati-Baouche, H. De Baynast, A. Lebert, S. Sun, C. J. S. Lopez-Mingo, P. Leclaire, P. Michaud, *Ind. Crops Prod.* **2014**, *58*, 244.
[22] Y. H. Jung, T.-H. Chang, H. Zhang, C. Yao, Q. Zheng, V. W. Yang, H. Mi, M. Kim, S. J. Cho, D.-W. Park, *Nat. Commun.* **2015**, *6*, 7170.
[23] M. Nogi, S. Iwamoto, A. N. Nakagaito, H. Yano, *Adv. Mater.* **2009**, *21*, 1595.
[24] Y. Zhou, C. Chen, S. Zhu, C. Sui, C. Wang, Y. Kuang, U. Ray, D. Liu, A. Brozena, U. H. Leiste, *Mater. Today* **2019**, *30*, 17.
[25] L. Nyholm, G. Nyström, A. Mihranyan, M. Strømme, *Adv. Mater.* **2011**, *23*, 3751.
[26] Z. Y. Wu, C. Li, H. W. Liang, J. F. Chen, S. H. Yu, *Angew. Chem., Int. Ed.* **2013**, *52*, 2925.
[27] Y. Zhu, S. Murali, W. Cai, X. Li, J. W. Suk, J. R. Potts, R. S. Ruoff, *Adv. Mater.* **2010**, *22*, 3906.
[28] J.-U. Park, S. Nam, M.-S. Lee, C. M. Lieber, *Nat. Mater.* **2012**, *11*, 120.
[29] M. Pumera, *Energy Environ. Sci.* **2011**, *4*, 668.
[30] R. Raccichini, A. Varzi, S. Passerini, B. Scrosati, *Nat. Mater.* **2015**, *14*, 271.
[31] T. Pirzada, Z. Ashrafi, W. Xie, S. A. Khan, *Adv. Funct. Mater.* **2020**, *30*, 1907359.
[32] Y. Deng, T. Shang, Z. Wu, Y. Tao, C. Luo, J. Liang, D. Han, R. Lyu, C. Qi, W. Lv, *Adv. Mater.* **2019**, *31*, 1902432.
[33] H.-P. Cong, X.-C. Ren, P. Wang, S.-H. Yu, *ACS Nano* **2012**, *6*, 2693.
[34] Y. Sun, J. Cheng, *Bioresour. Technol.* **2002**, *83*, 1.
[35] Y. H. P. Zhang, L. R. Lynd, *Biotechnol. Bioeng.* **2004**, *88*, 797.
[36] C. Lei, J. Gao, W. Ren, Y. Xie, S. Y. H. Abdalkarim, S. Wang, Q. Ni, J. Yao, *Carbohydr. Polym.* **2019**, *205*, 35.
[37] Y. Zhu, Y. Ogasawara, *Geology* **2002**, *30*, 947.
[38] T. R. Mattsson, J. M. D. Lane, K. R. Cochrane, M. P. Desjarlais, A. P. Thompson, F. Pierce, G. S. Grest, *Phys. Rev. B* **2010**, *81*, 054103.
[39] S. Plimpton, *J Comput. Phys.* **1995**, *117*, 1.
[40] A. Dasari, Z.-Z. Yu, G.-P. Cai, Y.-W. Mai, *Prog. Polym. Sci.* **2013**, *38*, 1357.
[41] T. Kashiwagi, F. Du, J. F. Douglas, K. I. Winey, R. H. Harris, J. R. Shields, *Nat. Mater.* **2005**, *4*, 928.
[42] C. He, J. Huang, S. Li, K. Meng, L. Zhang, Z. Chen, Y. Lai, *ACS Sustain. Chem. Eng.* **2018**, *6*, 927.
[43] K. Zhang, L. Zong, Y. Tan, Q. Ji, W. Yun, R. Shi, Y. Xia, *Carbohydr. Polym.* **2016**, *136*, 121.
[44] S. Qiu, Y. Zhou, X. Zhou, T. Zhang, C. Wang, R. K. K. Yuen, W. Hu, Y. Hu, *Small* **2019**, *15*, 1805175.
[45] S. Qiu, C. Ma, X. Wang, X. Zhou, X. Feng, R. K. Yuen, Y. Hu, *J. Hazard. Mater.* **2018**, *344*, 839.
[46] S. Qiu, X. Wang, B. Yu, X. Feng, X. Mu, R. K. Yuen, Y. Hu, *J. Hazard. Mater.* **2017**, *325*, 327.
[47] R. Shi, L. Tan, L. Zong, Q. Ji, X. Li, K. Zhang, L. Cheng, Y. Xia, *Carbohydr. Polym.* **2017**, *157*, 1594.
[48] X. Li, K. Zhang, R. Shi, X. Ma, L. Tan, Q. Ji, Y. Xia, *Carbohydr. Polym.* **2017**, *176*, 246.
[49] P. Collishaw, J. Evans, *J. Mater. Sci.* **1994**, *29*, 2261.
[50] A. Isogai, T. Saito, H. Fukuzumi, *Nanoscale* **2011**, *3*, 71.